

Structure, Crystallographic Sites, and Tunable Luminescence Properties of Eu²⁺ and Ce³⁺/Li⁺-Activated Ca_{1.65}Sr_{0.35}SiO₄ Phosphors

Zhiguo Xia,*† Shihai Miao,‡ Mingyue Chen,† Maxim S. Molokeev,§,|| and Quanlin Liu†

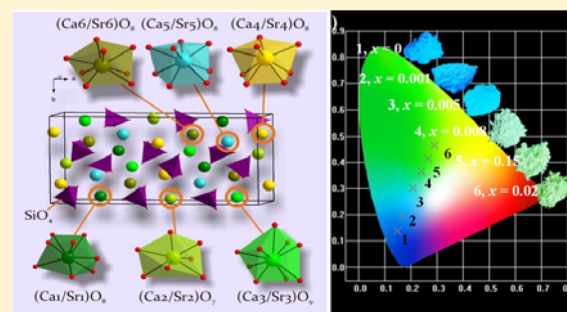
†School of Materials Sciences and Engineering, University of Science and Technology Beijing, Beijing 100083, China

‡School of Materials Sciences and Technology, China University of Geosciences, Beijing 100083, China

§Laboratory of Crystal Physics, Kirensky Institute of Physics, Siberian Branch of the Russian Academy of Sciences (SB RAS), Krasnoyarsk 660036, Russia

||Department of Physics, Far Eastern State Transport University, Khabarovsk 680021, Russia

ABSTRACT: Eu²⁺ and Ce³⁺/Li⁺ singly doped and Eu²⁺/Ce³⁺/Li⁺-codoped Ca_{1.65}Sr_{0.35}SiO₄ phosphors have been synthesized by a solid-state reaction method. The crystal structure was determined by Rietveld refinement to verify the formation of the α'_L-Ca₂SiO₄ phase with the Sr addition into Ca₂SiO₄, and the preferred crystallographic positions of the Eu²⁺ and Ce³⁺/Li⁺ ions in Ca_{1.65}Sr_{0.35}SiO₄ were analyzed based on a comparison of the unit-cell volumes and the designed chemical compositions of undoped isostructural compounds Ca_(2-x)Sr_xSiO₄ ($x = 0.25, 0.35, 0.45, 0.55$ and 0.65). Ce³⁺/Li⁺ singly activated Ca_{1.65}Sr_{0.35}SiO₄ phosphors exhibit strong absorption in the range of 250–450 nm and a blue emission peak centered at about 465 nm. When Eu²⁺ ions are codoped, the emission colors of Ca_{1.65}Sr_{0.35}SiO₄:Ce³⁺, Li⁺, Eu²⁺ phosphors under the irradiation of 365 nm can be finely tuned from blue to green through the energy transfer from Ce³⁺ to Eu²⁺. The involved energy-transfer process between Ce³⁺ and Eu²⁺ and the corresponding mechanism are discussed in detail. The reported Ca_{1.65}Sr_{0.35}SiO₄:Ce³⁺, Li⁺, Eu²⁺ phosphor might be a candidate for color-tunable blue-green components in the fabrication of near-ultraviolet-pumped white-light-emitting diodes (WLEDs).



1. INTRODUCTION

Rare-earth- (RE-) containing materials have attracted great interest for a wide variety of applications in the optical, magnetic, and electrical fields. In particular, RE-doped phosphor materials play an important role in the illumination and display industry, especially in terms of solid-state lighting (SSL) products based on white-light-emitting diodes (WLEDs).^{1–3} Currently, many phosphors can be used in WLEDs, including Ce³⁺- and Eu²⁺-doped oxide, nitride, oxynitride, and oxyfluoride compounds.³ A well-known commercial phosphor is yellow-emitting Y₃Al₅O₁₂:Ce³⁺ (YAG), which can be combined with a blue InGaN LED chip to fabricate the WLEDs. Ce³⁺- and Eu²⁺-doped metal nitrides and oxynitrides, such as Sr₂Si₅N₈:Eu²⁺ and CaAlSi-N₃:Eu²⁺, and Ce³⁺/Eu³⁺-codoped α-SiAlON phosphors also show excellent photoluminescence properties.^{3,4} Recently, silicate-based phosphors have been reported by several groups aiming at different research interests. Among them, orthosilicate phosphors with the general compositions of Eu²⁺- or Ce³⁺-doped A₂SiO₄ (A = Ca, Sr, Ba) have recently attracted much attention because of their low manufacturing costs, rigid crystal structures, abundant phase transformations, and tunable luminescence properties.^{2,5–8}

Eu²⁺ and Ce³⁺ ions are two significant activators for luminescent materials because of their unique emission properties, combining broad emission spectra that can lead to

good color-rendering properties; relatively small Stokes shifts that allow for excitation in the near-UV and blue parts of the spectrum; and short decay times, which avoid saturation effects.⁹ Accordingly, many Ce³⁺- and Eu²⁺-codoped phosphors have been reported, including Ba₃Si₆O₉N₄:Ce³⁺, Eu²⁺, Ca₈La₂(PO₄)₆O₂:Ce³⁺, Eu²⁺, and Li₂Si₂O₄:Eu²⁺, Ce³⁺.^{10–12} It was found that Eu²⁺ can be sensitized by Ce³⁺ in some select lattices because of the spectral overlap between the emission band of Ce³⁺ and the excitation band of Eu²⁺. Consequently, tunable emission can be produced in this type of Ce³⁺/Eu²⁺-codoped single-composition host.

Recently, Eu²⁺ and Ce³⁺ singly doped Ca₂SiO₄-based orthosilicate phosphors with multicolor emissions have drawn much attention. Only β-Ca₂SiO₄ and γ-Ca₂SiO₄ can be obtained at room temperature, although there are five polytypes, namely, α-Ca₂SiO₄, α'_L-Ca₂SiO₄, α'_H-Ca₂SiO₄, β-Ca₂SiO₄, and γ-Ca₂SiO₄. Herein, we show that the introduction of Sr²⁺ can be used to stabilize the high-temperature phase of Ca₂SiO₄, giving Ca_{1.65}Sr_{0.35}SiO₄ isostructural to α'_L-Ca₂SiO₄. The luminescence properties of Ce³⁺- and Eu²⁺-activated Ca_{1.65}Sr_{0.35}SiO₄ phosphors have not previously been reported. Our focus in this work was to understand the crystal structure of the Ca_{1.65}Sr_{0.35}SiO₄ phase, the preferred crystallographic

Received: February 25, 2015

Published: June 11, 2015

positions of the Eu^{2+} and $\text{Ce}^{3+}/\text{Li}^+$ ions in the $\text{Ca}_{1.65}\text{Sr}_{0.35}\text{SiO}_4$ host, and the tunable emission of $\text{Ca}_{1.65}\text{Sr}_{0.35}\text{SiO}_4:\text{Ce}^{3+}, \text{Li}^+, \text{Eu}^{2+}$ phosphors. The involved energy-transfer process between Ce^{3+} and Eu^{2+} is also discussed in detail. According to the results of comparative investigations of the photoluminescence (PL) and photoluminescence excitation (PLE) spectra, fluorescence lifetimes, and CIE chromaticity coordinates, the emission color can be tuned from blue to green depending on the relative $\text{Ce}^{3+}/\text{Eu}^{2+}$ concentrations.

2. EXPERIMENTAL SECTION

2.1. Materials and Synthesis. The starting materials CeO_2 (99.99%) and Eu_2O_3 (99.99%) were supplied by China Mines (Beijing) Research Institute, Beijing, China, and CaCO_3 (99.5%), SrCO_3 (99.5%), Li_2CO_3 (99.5%) and SiO_2 (99.5%) were purchased from Sinopharm Chemical Reagent Co. Ltd., Shanghai, China. The designed phosphors with nominal compositions of $\text{Ca}_{1.65-2x}\text{Sr}_{0.35}\text{SiO}_4:x\text{Ce}^{3+}, x\text{Li}^+$, $\text{Ca}_{1.65}\text{Sr}_{0.35-y}\text{SiO}_4:y\text{Eu}^{2+}$, and $\text{Ca}_{1.65-2x}\text{Sr}_{0.35-y}\text{SiO}_4:x\text{Ce}^{3+}, x\text{Li}^+, y\text{Eu}^{2+}$ were synthesized by the conventional high-temperature solid-state reaction method. According to the selected stoichiometric compositions, the weighed starting materials were mixed and ground in an agate mortar for 15 min; then, the mixture was placed in a crucible and sintered at 1400 °C for 5 h in a reducing atmosphere of H_2 (10%) and N_2 (90%) to produce the samples. The prepared phosphors were cooled to room temperature and then reground for further measurements.

2.2. Measurements and Characterization. Powder X-ray diffraction (XRD) measurements were performed on a D8 ADVANCE diffractometer (Bruker AXS GmbH, Karlsruhe, Germany) operating at 40 kV and 40 mA with $\text{Cu K}\alpha$ radiation ($\lambda = 1.5406 \text{ \AA}$). The scanning rate was fixed at 4°/min with 2θ ranges from 10° to 70° for phase identification, and the data for Rietveld analysis were collected in step-scanning mode with a step size of 0.02° and a counting time of 10 s per step over the 2θ range from 10° to 120°. The elemental content analysis was performed by inductively coupled plasma optical emission spectrometry (ICP-OES) using an iCAP 6300 spectrometer (Thermo Fisher Scientific, Waltham, MA). Photoluminescence (PL) emission and photoluminescence excitation (PLE) spectra were measured on a Hitachi F-4600 spectrophotometer equipped with a 150-W xenon lamp as the excitation source. Decay curves were recorded on an Edinburgh Instruments FLSP920 spectrometer with an nF900 flash lamp used as the excitation resource. Quantum efficiency was measured using an integrating sphere on the same FLSP920 fluorescence spectrophotometer. All measurements were performed at room temperature.

3. RESULTS AND DISCUSSION

3.1. Phase and Crystallographic Site Analysis. XRD patterns of the as-prepared $\text{Ca}_{1.65-2x}\text{Sr}_{0.35-y}\text{SiO}_4:x\text{Ce}^{3+}, x\text{Li}^+, y\text{Eu}^{2+}$ phosphors were collected to verify the phase purity. In Figure 1 are shown the XRD patterns of $\text{Ca}_{1.59}\text{Sr}_{0.35}\text{SiO}_4:0.03\text{Ce}^{3+}, 0.03\text{Li}^+$, $\text{Ca}_{1.65}\text{Sr}_{0.345}\text{SiO}_4:0.005\text{Eu}^{2+}$, and $\text{Ca}_{1.59}\text{Sr}_{0.345}\text{SiO}_4:0.03\text{Ce}^{3+}, 0.03\text{Li}^+, 0.005\text{Eu}^{2+}$, along with the standard pattern for $\text{Ca}_{1.65}\text{Sr}_{0.35}\text{SiO}_4$ (JCPDS 77-399) as a reference. One can see that all of the diffraction peaks of the selected samples can be indexed to the corresponding standard data for $\text{Ca}_{1.65}\text{Sr}_{0.35}\text{SiO}_4$ (JCPDS 77-399), suggesting the phase purity of the as-prepared samples. Thus, the doped ions do not give rise to any impurity or possible phase transition. To further understand the crystal structure of $\text{Ca}_{1.65}\text{Sr}_{0.35}\text{SiO}_4$, Figure 2 presents difference Rietveld plots for $\text{Ca}_{1.65}\text{Sr}_{0.25}\text{SiO}_4:0.10\text{Eu}^{2+}$ and $\text{Ca}_{1.45}\text{Sr}_{0.35}\text{SiO}_4:0.10\text{Ce}^{3+}, 0.10\text{Li}^+$, and the main parameters from the processing and refinement of the data are reported in Table 1. Rietveld refinement was performed using TOPAS 4.2 software, and it was found that almost all peaks were indexed to an orthorhombic cell ($Pna2_1$) with parameters close to those of

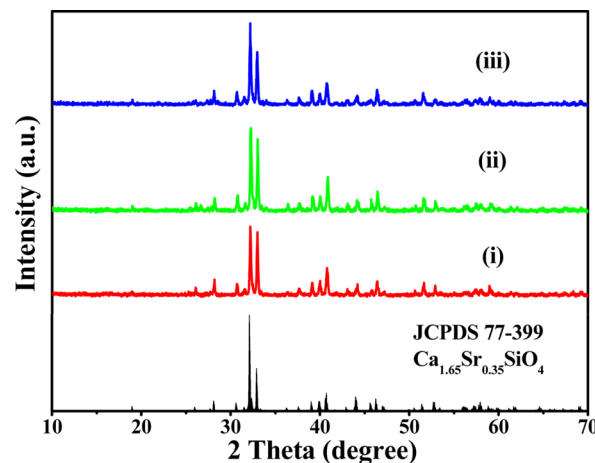


Figure 1. XRD patterns of as-prepared (i) $\text{Ca}_{1.59}\text{Sr}_{0.35}\text{SiO}_4:0.03\text{Ce}^{3+}, 0.03\text{Li}^+$, (ii) $\text{Ca}_{1.65}\text{Sr}_{0.345}\text{SiO}_4:0.005\text{Eu}^{2+}$, and (iii) $\text{Ca}_{1.59}\text{Sr}_{0.345}\text{SiO}_4:0.03\text{Ce}^{3+}, 0.03\text{Li}^+, 0.005\text{Eu}^{2+}$. The standard pattern for $\text{Ca}_{1.65}\text{Sr}_{0.35}\text{SiO}_4$ (JCPDS 77-399) is shown as a reference.

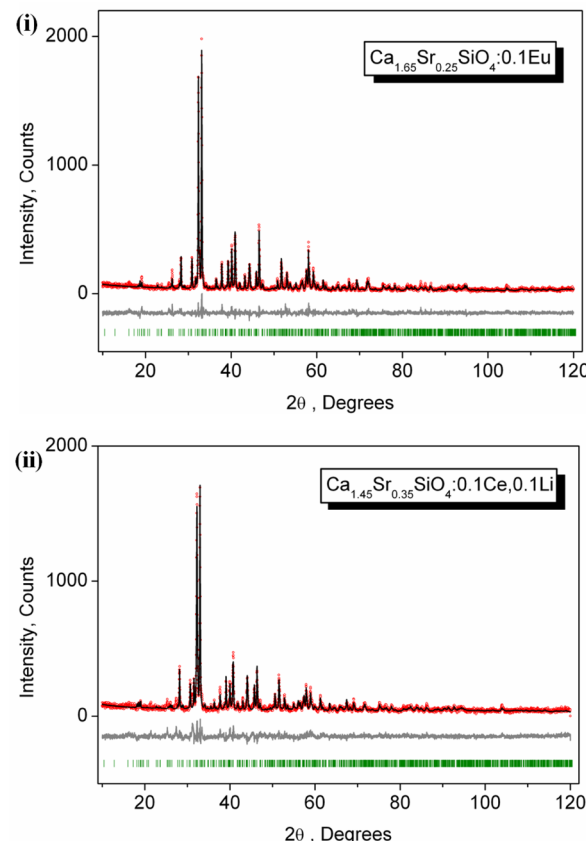


Figure 2. Difference Rietveld plots of (i) $\text{Ca}_{1.65}\text{Sr}_{0.25}\text{SiO}_4:0.10\text{Eu}^{2+}$ and (ii) $\text{Ca}_{1.45}\text{Sr}_{0.35}\text{SiO}_4:0.10\text{Ce}^{3+}, 0.10\text{Li}^+$.

the Ca_2SiO_4 phase (ICSD-82996).^{13,14} Ca_2SiO_4 is known to exhibit several crystal structures, namely, α - Ca_2SiO_4 , α'_L - Ca_2SiO_4 , α'_H - Ca_2SiO_4 , β - Ca_2SiO_4 , and γ - Ca_2SiO_4 , where the first three polymorphs are high-temperature phases and the last two can be stabilized at room temperature.¹³ The γ phase is generally synthesized at a higher temperature than β phase because of its thermodynamically more stable crystal structure. Recent studies showed that the addition of some ions, such as

Table 1. Main Parameters from the Processing and Refinement of $\text{Ca}_{1.65}\text{Sr}_{0.25}\text{SiO}_4:\text{0.10Eu}^{2+}$ and $\text{Ca}_{1.45}\text{Sr}_{0.35}\text{SiO}_4:\text{0.10Ce}^{3+},\text{0.10Li}^+$ Samples

	$\text{Ca}_{1.65}\text{Sr}_{0.25}\text{SiO}_4:\text{0.10Eu}^{2+}$	$\text{Ca}_{1.45}\text{Sr}_{0.35}\text{SiO}_4:\text{0.10Ce}^{3+},\text{0.10Li}^+$
space group	$Pna2_1$	$Pna2_1$
a (Å)	20.464(2)	20.541(2)
b (Å)	9.3182(9)	9.3490(9)
c (Å)	5.5481(5)	5.5534(5)
V (Å ³)	1057.97(17)	1066.46(19)
2θ interval (deg)	10–120	10–120
no. of reflections	889	897
no. of refined params	118	99
R_{wp} (%)	16.31	16.98
R_p (%)	12.38	12.38
R_{exp} (%)	12.98	11.77
χ^2	1.26	1.44
R_B (%)	4.75	5.78

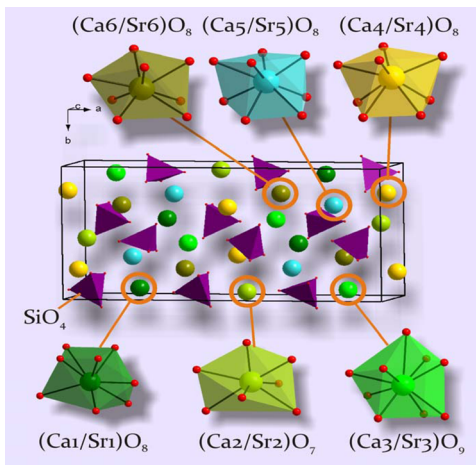


Figure 3. Structural view of a unit cell of $\text{Ca}_{1.65}\text{Sr}_{0.35}\text{SiO}_4$ and coordination environments for Ca/Sr sites.

RE ions (Ce^{3+}) or other codopants (Al^{3+}), can induce the phase transformation between $\beta\text{-Ca}_2\text{SiO}_4$ and $\gamma\text{-Ca}_2\text{SiO}_4$.

In the present case, the crystalline phase of the as-prepared $\text{Ca}_{1.65-2x}\text{Sr}_{0.35-y}\text{SiO}_4:x\text{Ce}^{3+},y\text{Li}^+,y\text{Eu}^{2+}$ phosphors should be the same as that of the high-temperature $\alpha'_L\text{-Ca}_2\text{SiO}_4$ phase, and we believe that the addition of Sr^{2+} to Ca_2SiO_4 resulted in the formation of the $\alpha'_L\text{-Ca}_2\text{SiO}_4$ phase with the nominal composition of $\text{Ca}_{1.65}\text{Sr}_{0.35}\text{SiO}_4$. Such a high-temperature phase can be stabilized as a result of an increase in cell volume from $\text{Sr}^{2+}/\text{Ca}^{2+}$ substitution. Therefore, the $\alpha'_L\text{-Ca}_2\text{SiO}_4$ (ICSD-82996) crystal structure was taken as a starting model for Rietveld refinement. The structure has 6 independent Ca positions, 3 Si positions, and 12 O positions, and crystal structure refinement from powder data is a complex task. However, it is almost impossible to locate Sr^{2+} ions in specific Ca^{2+} sites. Therefore, during the refinement, the Ca^{2+} sites were assumed to be occupied by Sr^{2+} with a fixed occupation according to chemical formula. Nevertheless, the present model gave a stable refinement and low R factors. Accordingly, Figure 3 displays the $\text{Ca}_{1.65}\text{Sr}_{0.35}\text{SiO}_4$ unit cell and coordination environment for the $\text{Ca}^{2+}/\text{Sr}^{2+}$ sites. Ca^{2+} and Sr^{2+} are known to have the same coordination environment. In the $\text{Ca}_{1.65}\text{Sr}_{0.35}\text{SiO}_4$ host, there are six types of $\text{Ca}^{2+}/\text{Sr}^{2+}$ sites, which are denoted as Ca1/Sr1, Ca2/Sr2, Ca3/Sr3, Ca4/Sr4, Ca5/Sr5, and Ca6/Sr6 here for easier identification. The Ca1/Sr1, Ca4/Sr4, Ca5/Sr5, and Ca6/Sr6 sites are coordinated by eight oxygen atoms, whereas the Ca2/Sr2 site is coordinated by seven oxygen atoms and the Ca3/Sr3 site is coordinated by nine oxygen atoms. The cations in the host lattice are connected by $[\text{SiO}_4]^{4-}$ tetrahedra. We also performed an ICP analysis of the $\text{Ca}_{1.59}\text{Sr}_{0.27}\text{SiO}_4:0.03\text{Ce}^{3+},0.03\text{Li}^+,0.08\text{Eu}^{2+}$ sample, measuring element contents for Ca, Sr, Si, Ce, Eu, and Li of 33.76%, 15.42%, 12.07%, 1.739%, 1.426%, and 0.0283%, respectively, compared to theoretical contents of 33.16%, 15.04%, 14.62%, 2.19%, 1.58%, and 0.108%, respectively. The

Table 2. Main Parameters from the Refinement of the Undoped Samples $\text{Ca}_{2-x}\text{Sr}_x\text{SiO}_4$ ($x = 0.25, 0.35, 0.45, 0.55$, and 0.65)

	$\text{Ca}_{1.75}\text{Sr}_{0.25}\text{SiO}_4$	$\text{Ca}_{1.65}\text{Sr}_{0.35}\text{SiO}_4$	$\text{Ca}_{1.55}\text{Sr}_{0.45}\text{SiO}_4$	$\text{Ca}_{1.45}\text{Sr}_{0.55}\text{SiO}_4$	$\text{Ca}_{1.35}\text{Sr}_{0.65}\text{SiO}_4$
space group	$Pna2_1$	$Pna2_1$	$Pna2_1$	$Pna2_1$	$Pna2_1$
a (Å)	20.393(2)	20.476(2)	20.531(2)	20.648(5)	20.660(4)
b (Å)	9.3106(9)	9.3299(9)	9.348(1)	9.397(2)	9.3892(16)
c (Å)	5.5478(5)	5.5551(5)	5.5600(6)	5.5679(13)	5.567(1)
V (Å ³)	1053.4(2)	1061.2(2)	1067.0(2)	1080.3(5)	1080.4(3)
2θ range (deg)	10–120	10–120	10–120	10–120	10–120
R_p (%)	12.23	11.74	11.66	10.46	10.28
χ^2	1.56	1.54	1.67	1.82	1.60

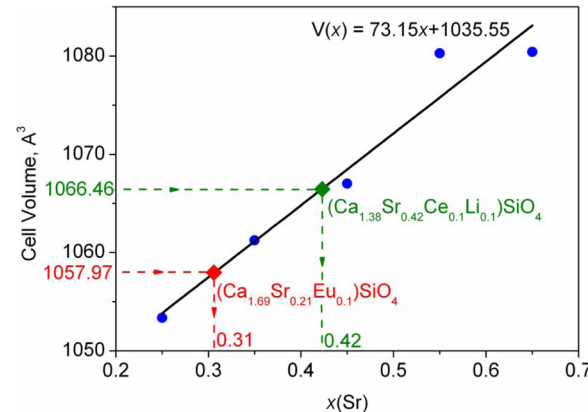


Figure 4. Cell volumes of the series $\text{Ca}_{(2-x)}\text{Sr}_x\text{SiO}_4$, with $x = 0.25, 0.35, 0.45, 0.55, 0.65$ (blue circles) and linear fitting $V(x)$ of their values per x (black line). The concentration of $(\text{Sr} + \text{Eu})$ ions in $(\text{Ca}_{1.69}\text{Sr}_{0.21}\text{Eu}_{0.1})\text{SiO}_4$ was found by using the intersection (red value and line) with $V(x)$. The concentration of Sr was calculated from this value assuming a fixed concentration of Eu equal to 0.1. The concentration of Sr ions in $(\text{Ca}_{1.38}\text{Sr}_{0.42}\text{Ce}_{0.1}\text{Li}_{0.1})\text{SiO}_4$ was found by using the intersection (green value and line) with $V(x)$.

82996) crystal structure was taken as a starting model for Rietveld refinement. The structure has 6 independent Ca positions, 3 Si positions, and 12 O positions, and crystal structure refinement from powder data is a complex task. However, it is almost impossible to locate Sr^{2+} ions in specific Ca^{2+} sites. Therefore, during the refinement, the Ca^{2+} sites were assumed to be occupied by Sr^{2+} with a fixed occupation according to chemical formula. Nevertheless, the present model gave a stable refinement and low R factors. Accordingly, Figure 3 displays the $\text{Ca}_{1.65}\text{Sr}_{0.35}\text{SiO}_4$ unit cell and coordination environment for the $\text{Ca}^{2+}/\text{Sr}^{2+}$ sites. Ca^{2+} and Sr^{2+} are known to have the same coordination environment. In the $\text{Ca}_{1.65}\text{Sr}_{0.35}\text{SiO}_4$ host, there are six types of $\text{Ca}^{2+}/\text{Sr}^{2+}$ sites, which are denoted as Ca1/Sr1, Ca2/Sr2, Ca3/Sr3, Ca4/Sr4, Ca5/Sr5, and Ca6/Sr6 here for easier identification. The Ca1/Sr1, Ca4/Sr4, Ca5/Sr5, and Ca6/Sr6 sites are coordinated by eight oxygen atoms, whereas the Ca2/Sr2 site is coordinated by seven oxygen atoms and the Ca3/Sr3 site is coordinated by nine oxygen atoms. The cations in the host lattice are connected by $[\text{SiO}_4]^{4-}$ tetrahedra. We also performed an ICP analysis of the $\text{Ca}_{1.59}\text{Sr}_{0.27}\text{SiO}_4:0.03\text{Ce}^{3+},0.03\text{Li}^+,0.08\text{Eu}^{2+}$ sample, measuring element contents for Ca, Sr, Si, Ce, Eu, and Li of 33.76%, 15.42%, 12.07%, 1.739%, 1.426%, and 0.0283%, respectively, compared to theoretical contents of 33.16%, 15.04%, 14.62%, 2.19%, 1.58%, and 0.108%, respectively. The

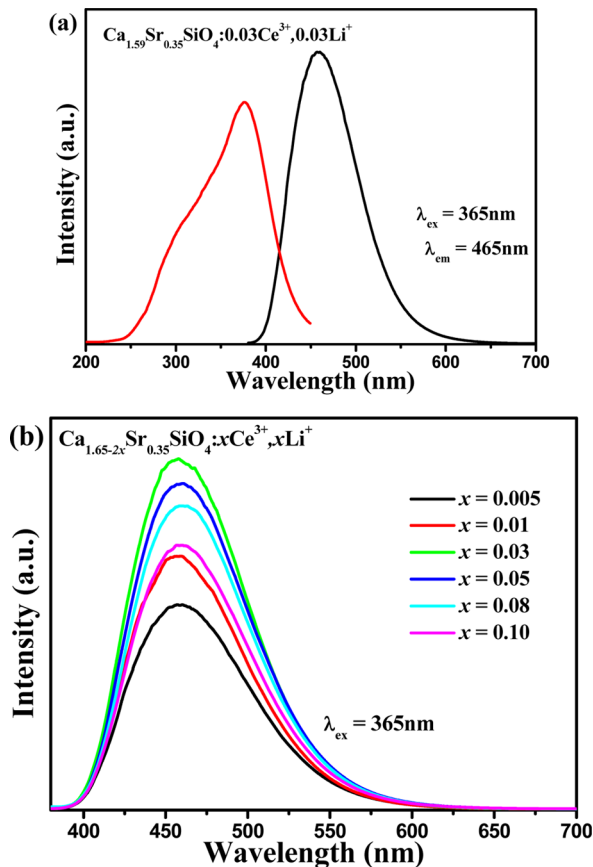


Figure 5. (a) PLE and PL spectra of $\text{Ca}_{1.59}\text{Sr}_{0.35}\text{SiO}_4:0.03\text{Ce}^{3+},0.03\text{Li}^+$, (b) PL spectra of $\text{Ca}_{1.65-x}\text{Sr}_{0.35}\text{SiO}_4:xCe^{3+},x\text{Li}^+$ ($x = 0.005, 0.01, 0.03, 0.05, 0.08, 0.10$).

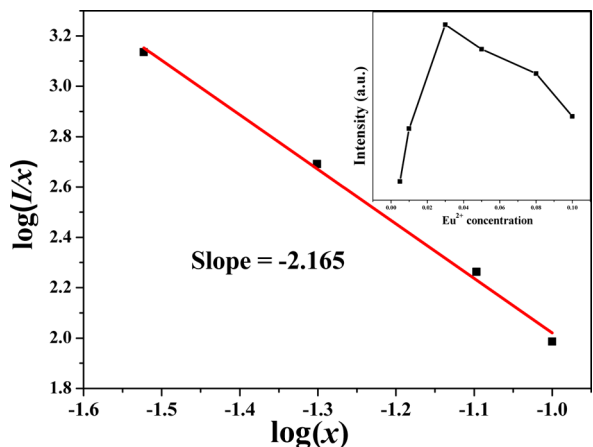


Figure 6. Relationship of $\log(x)$ versus $\log(I/x)$ for $\text{Ca}_{1.65-x}\text{Sr}_{0.35}\text{SiO}_4:xCe^{3+},x\text{Li}^+$ phosphors. Inset: PL intensity as a function of Ce³⁺ content.

two sets of values agree well, and the results verify the chemical composition and the concentrations of doping ions.

It is known that the doping of functional materials by cations or anions is very important for the modification of their physical properties. Thus, the evaluation of preferred crystallographic sites for dopant incorporation is of fundamental scientific interest, as it will shed light on efficient ways to further modify the properties of the applied materials. Herein, the preferred crystallographic positions of the Eu²⁺ and Ce³⁺/

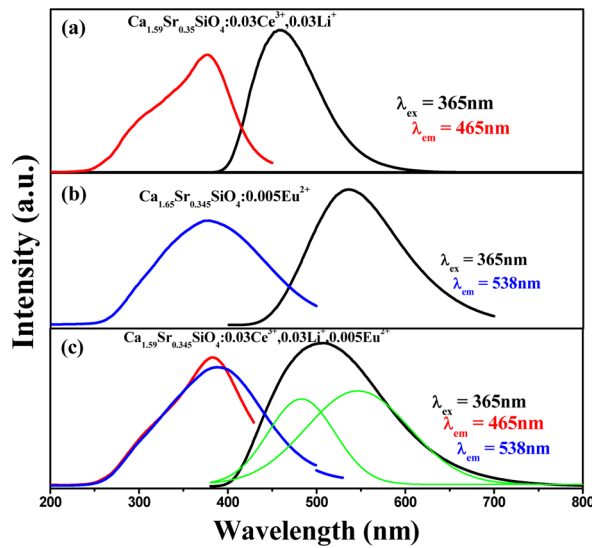


Figure 7. (Left) PLE and (right) PL spectra of (a) $\text{Ca}_{1.59}\text{Sr}_{0.35}\text{SiO}_4:0.03\text{Ce}^{3+},0.03\text{Li}^+$, (b) $\text{Ca}_{1.65}\text{Sr}_{0.345}\text{SiO}_4:0.005\text{Eu}^{2+}$, and (c) $\text{Ca}_{1.59}\text{Sr}_{0.345}\text{SiO}_4:0.03\text{Ce}^{3+},0.03\text{Li}^+,0.005\text{Eu}^{2+}$.

Li^+ ions in the $\text{Ca}_{1.65}\text{Sr}_{0.35}\text{SiO}_4$ host were analyzed. The identification of the positions of the Eu²⁺ and Ce³⁺/Li⁺ ions in the relatively complex $\text{Ca}_{1.65}\text{Sr}_{0.35}\text{SiO}_4$ host is a challenge for understanding structure–property relationships. Although the specific concentrations of $\text{Ca}^{2+}/\text{Sr}^{2+}$ in the host and the doped Eu²⁺ and Ce³⁺/Li⁺ ions cannot be refined directly, the concentrations of $\text{Ca}^{2+}/\text{Sr}^{2+}$ ions in the designed isostructural $\text{Ca}_{(2-x)}\text{Sr}_x\text{SiO}_4$ compounds can be estimated from the cell volumes assuming fixed concentrations of Eu²⁺ and Ce³⁺/Li⁺. That is, if the Eu²⁺-doped compound and the undoped compound $\text{Ca}_{2-x}\text{Sr}_x\text{SiO}_4$ have the same cell volumes, then the concentrations of Ca^{2+} ions in the two compounds should be nearly the same because ion radius (IR) of Sr²⁺ [coordination number (CN) = 8, IR = 1.26 Å] is close to IR of Eu²⁺ (CN = 8, IR = 1.25 Å).¹⁵ On the other hand, the total concentration of Sr²⁺ + Eu²⁺ in the doped compound should be similar to the concentration of Sr²⁺ in the undoped compound in this case. Similarly, if the Ce³⁺/Li⁺-doped compound has the same cell volume as some other undoped compound $\text{Ca}_{2-x}\text{Sr}_x\text{SiO}_4$, then the concentrations of Sr²⁺ in the two compounds should be similar because the average IR can be calculated as $(0.92 \text{ \AA} + 1.143 \text{ \AA})/2 = 1.03 \text{ \AA}$ (CN = 6, IR_{Li⁺} = 0.92 Å, IR_{Ce³⁺} = 1.143 Å), which is close to IR of Ca²⁺ (CN = 8, IR = 1.12 Å).¹⁵ Thus, we designed and prepared a series of undoped $\text{Ca}_{(2-x)}\text{Sr}_x\text{SiO}_4$, ($x = 0.25, 0.35, 0.45, 0.55, 0.65$) compounds and conducted Le Bail profile fitting for this series of compounds using TOPAS 4.2. Table 2 lists the main parameters from the processing and refinement of the undoped $\text{Ca}_{2-x}\text{Sr}_x\text{SiO}_4$ ($x = 0.25, 0.35, 0.45, 0.55, 0.65$) samples. Figure 4 shows the cell volumes of the $\text{Ca}_{2-x}\text{Sr}_x\text{SiO}_4$ ($x = 0.25, 0.35, 0.45, 0.55, 0.65$) samples obtained after refinement (blue circles in Figure 4), which were found to fulfill a linear relationship based on Vegard's law for this series: $V(x) = 73.15x + 1035.55 \text{ \AA}^3$ (black line in Figure 4). The cell-volume data for (i) $\text{Ca}_{1.65}\text{Sr}_{0.35}\text{SiO}_4:0.10\text{Eu}^{2+}$ and (ii) $\text{Ca}_{1.45}\text{Sr}_{0.35}\text{SiO}_4:0.10\text{Ce}^{3+},0.10\text{Li}^+$ obtained by Rietveld refinement (Figure 2 and Table 2) were used to evaluate the distributions of the Ca²⁺, Sr²⁺, Eu²⁺, and Ce³⁺/Li⁺ ions. The concentration of Sr²⁺ + Eu²⁺ in compound (i), 0.31, was found by using the intersection of its cell volume (1057.97) with $V(x)$

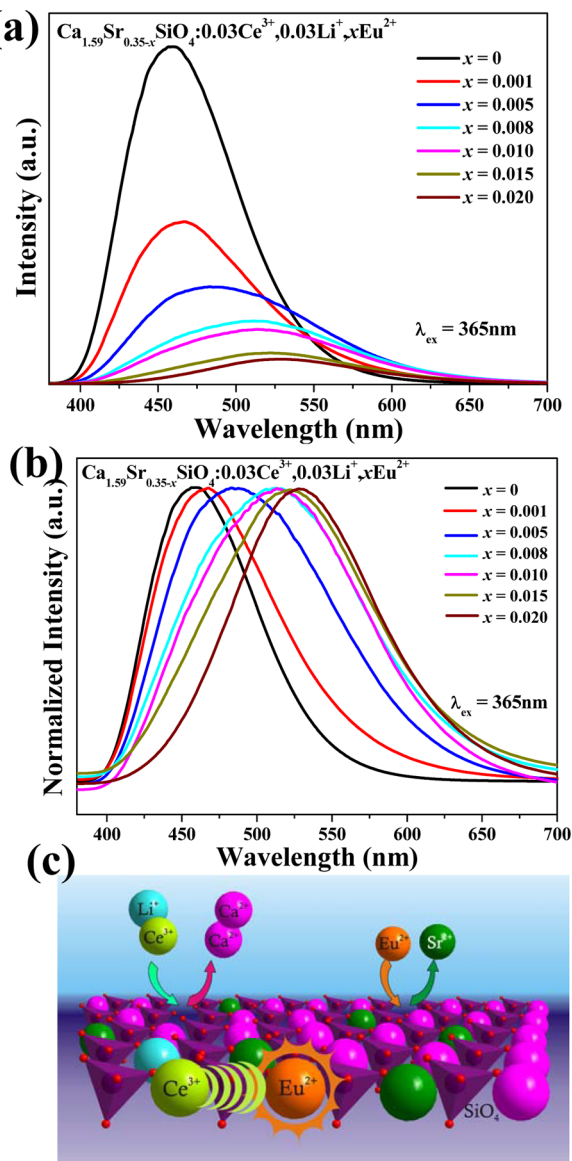


Figure 8. (a) As-measured and (b) normalized PL spectra of $\text{Ca}_{1.59}\text{Sr}_{0.35-x}\text{SiO}_4:0.03\text{Ce}^{3+},0.03\text{Li}^+,x\text{Eu}^{2+}$ ($x = 0, 0.001, 0.005, 0.008, 0.010, 0.015$, and 0.020) phosphors under 365-nm excitation. (c) Schematic illustration of the energy-transfer mechanism of the emission center in the matrix.

(red text and lines in Figure 4). From this value, it was concluded that the chemical formula of compound (i) should be $(\text{Ca}_{1.69}\text{Sr}_{0.21}\text{Eu}_{0.1})\text{SiO}_4$, which is close to the assumed formula of $(\text{Ca}_{1.65}\text{Sr}_{0.25}\text{Eu}_{0.1})\text{SiO}_4$. Similarly, the concentration of Sr²⁺ in compound (ii), 0.42, was found by using the intersection of its cell volume (1066.46) with $V(x)$ (green text and lines in Figure 4). Therefore, it was concluded that the chemical formula of compound (ii) should be $(\text{Ca}_{1.38}\text{Sr}_{0.42}\text{Ce}_{0.1}\text{Li}_{0.1})\text{SiO}_4$, which is also close to the assumed formula of $(\text{Ca}_{1.45}\text{Sr}_{0.35}\text{Ce}_{0.1}\text{Li}_{0.1})\text{SiO}_4$. Based on this model, we compared the cell volumes of the RE-doped phosphor materials and the isostructural compounds with different chemical compositions, and in this way, we were able to determine the preferred crystallographic sites of the dopants in this complex system.

3.2. Photoluminescence Properties of Ce³⁺/Li⁺-Doped $\text{Ca}_{1.65}\text{Sr}_{0.35}\text{SiO}_4$ Phosphors.

The PL and PLE spectra of

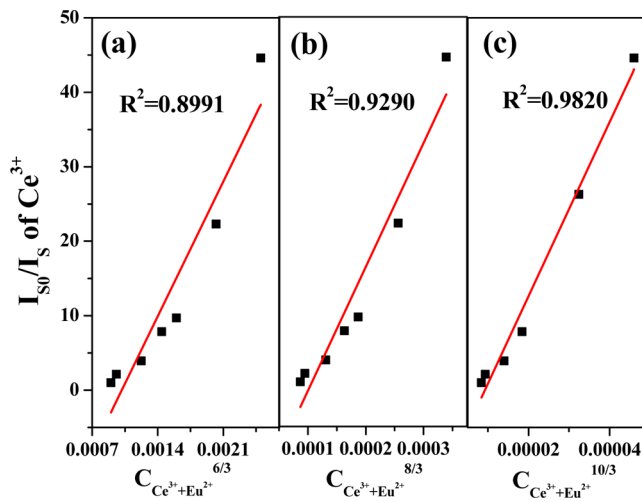


Figure 9. Dependence of I_{50}/I_5 of Ce³⁺ on (a) $C^{6/3}$, (b) $C^{8/3}$, and (c) $C^{10/3}$ derived from the $\text{Ca}_{1.59}\text{Sr}_{0.35-x}\text{SiO}_4:0.03\text{Ce}^{3+},0.03\text{Li}^+,x\text{Eu}^{2+}$ ($x = 0, 0.001, 0.005, 0.008, 0.010, 0.015$, and 0.020) phosphors.

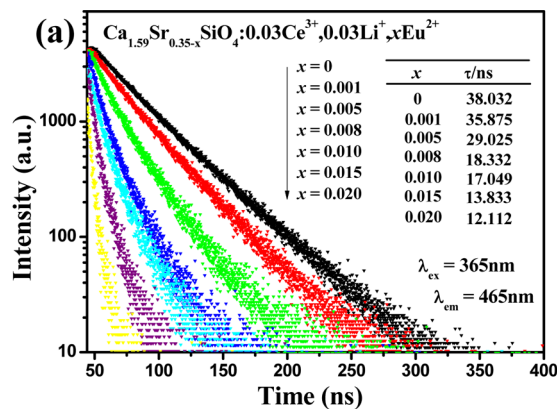


Figure 10. (a) Decay curves of Ce³⁺ emission in $\text{Ca}_{1.59}\text{Sr}_{0.35-x}\text{SiO}_4:0.03\text{Ce}^{3+},0.03\text{Li}^+,x\text{Eu}^{2+}$ phosphors under excitation at 365 nm. (b) Dependences of the Ce³⁺ fluorescence lifetime and energy-transfer efficiency on the doped Eu²⁺ molar concentration in $\text{Ca}_{1.59}\text{Sr}_{0.35-x}\text{SiO}_4:0.03\text{Ce}^{3+},0.03\text{Li}^+,x\text{Eu}^{2+}$ samples, monitored at 465 nm.

$\text{Ca}_{1.59}\text{Sr}_{0.35}\text{SiO}_4:0.03\text{Ce}^{3+},0.03\text{Li}^+$ are shown in Figure 5a. The PLE spectrum monitored at 465 nm exhibits a broad band from 250 to 450 nm, which corresponds to the transitions from the ground state of the Ce³⁺ ions to the field-splitting levels of the Sd state and also matches well with the near-UV chip for WLED applications.^{16,17} Upon excitation at 365 nm, the

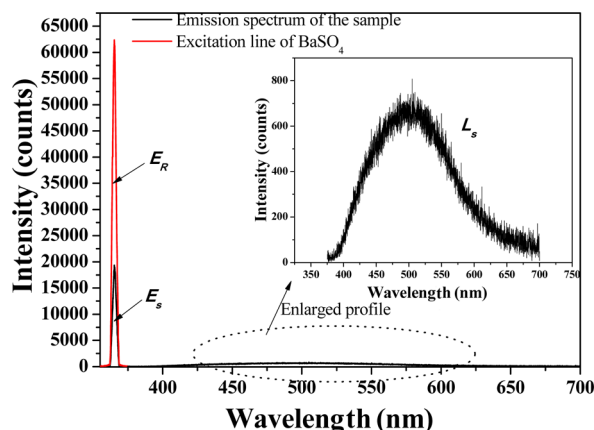


Figure 11. Excitation line of BaSO_4 and emission spectrum of the selected $\text{Ca}_{1.59}\text{Sr}_{0.27}\text{SiO}_4:0.03\text{Ce}^{3+},0.03\text{Li}^+,0.08\text{Eu}^{2+}$ phosphor collected using an integrating sphere. The inset shows a magnification of the emission spectrum.

emission spectrum shows a broad band peaking at 465 nm. Figure 5b presents the PL spectra of $\text{Ca}_{1.65-2x}\text{SrSiO}_4:x\text{Ce}^{3+},x\text{Li}^+$ ($x = 0.005, 0.01, 0.03, 0.05, 0.08$, and 0.10). It can be seen that the emission spectra consist of an asymmetric broad band centered at 465 nm, which corresponds to the 5d–4f allowed transition of Ce^{3+} . It can be easily seen that the emission intensity exhibits an obvious increasing trend with increasing Ce^{3+} concentration and maximizes at $x = 0.03$, after which it decreases, which can be ascribed to an internal concentration quenching effect.

The relationship of $\log(x)$ versus $\log(I/x)$ is shown in Figure 6. The inset shows the PL intensity of $\text{Ca}_{1.65-2x}\text{Sr}_{0.35}\text{SiO}_4:x\text{Ce}^{3+},x\text{Li}^+$

Table 3. Comparison of the CIE Chromaticity Coordinates (x, y) for $\text{Ca}_{1.59}\text{Sr}_{0.35-x}\text{SiO}_4:0.03\text{Ce}^{3+},0.03\text{Li}^+,x\text{Eu}^{2+}$ ($x = 0, 0.001, 0.005, 0.008, 0.015, 0.020$) Phosphors Excited at 365 nm

sample no.	sample composition (y)	CIE coordinates (x, y)
1	0	(0.148, 0.138)
2	0.001	(0.168, 0.196)
3	0.005	(0.208, 0.302)
4	0.008	(0.241, 0.365)
5	0.015	(0.265, 0.415)
6	0.020	(0.289, 0.466)

$\text{Ce}^{3+},x\text{Li}^+$ as a function of Ce^{3+} content. As mentioned above, the $\text{Ca}_{1.59}\text{Sr}_{0.35}\text{SiO}_4:0.03\text{Ce}^{3+},0.03\text{Li}^+$ phosphor has the strongest blue emission. In general, a concentration quenching effect can be caused by nonradiative energy transfer between activator ions and energy transfer of activator ions to impurities, color centers, or any other quenching centers. According to Van Uitert, if energy transfer occurs among the same type of activators, the intensity of the multipolar interaction can be determined from the change in the emission intensity from the emitting level that has the multipolar interaction. The emission intensity (I) per activator ion can be expressed as^{18,19}

$$\frac{I}{x} = K[1 + \beta(x)^{\theta/3}]^{-1} \quad (1)$$

where x is the concentration of the activator ions above the quenching concentration; I is the emission intensity; K and β are constants for a given host under the same excitation conditions; and θ has values of 6, 8, and 10 for dipole–dipole, dipole–quadrupole, and quadrupole–quadrupole interactions, respectively. To obtain the correct θ value, the dependence of

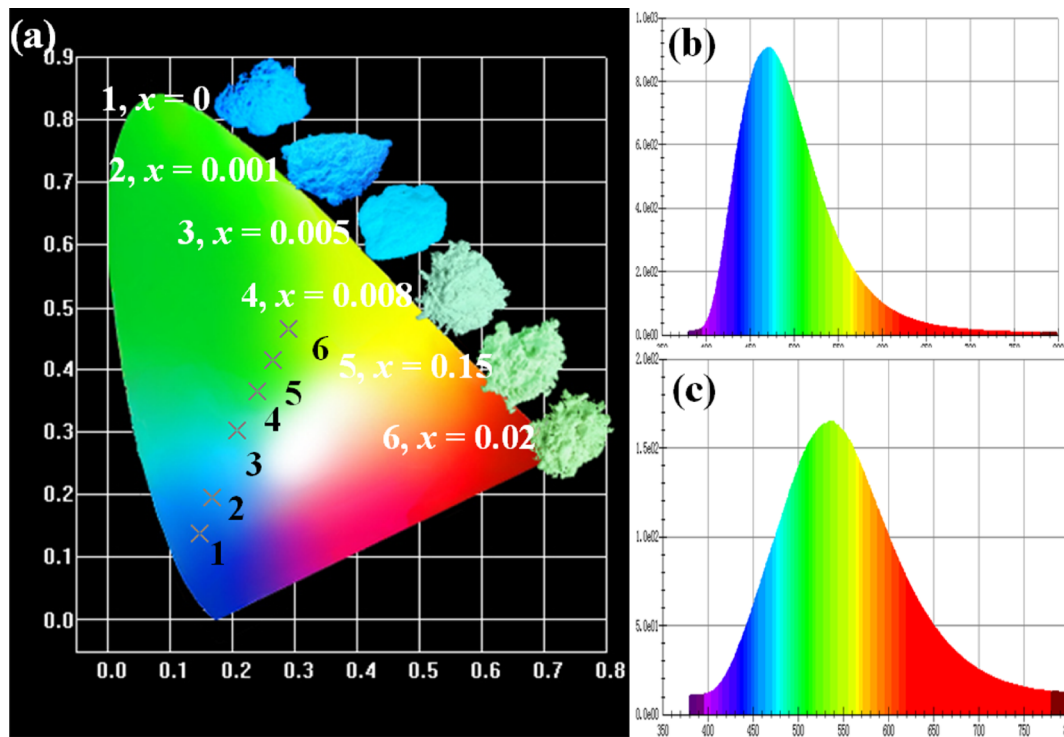


Figure 12. (a) CIE chromaticity diagram and a series of digital photographs of the selected $\text{Ca}_{1.59}\text{Sr}_{0.35-x}\text{SiO}_4:0.03\text{Ce}^{3+},0.03\text{Li}^+,x\text{Eu}^{2+}$ ($x = 0, 0.001, 0.005, 0.008, 0.015, 0.020$) phosphors ($\lambda_{\text{ex}} = 365$ nm). (b,c) Magnifications of the emission spectra of (b) $\text{Ca}_{1.59}\text{Sr}_{0.35}\text{SiO}_4:0.03\text{Ce}^{3+},0.03\text{Li}^+$ and (c) $\text{Ca}_{1.59}\text{Sr}_{0.33}\text{SiO}_4:0.03\text{Ce}^{3+},0.03\text{Li}^+,0.02\text{Eu}^{2+}$, showing the differences in the emission spectra.

$\log(I/x)$ on $\log(x)$ is plotted and yields a straight line with a slope equal to $-\theta/3$. Therefore, Figure 6 shows the relationship of $\log(I/x)$ to $\log(x)$ to understand the concentration quenching. Based on the results in Figure 6, the slope is -2.165 , and the value of θ can be calculated as 6.5 , which is approximately equal to 6 . This means that the concentration quenching can be ascribed to dipole–dipole (d–d) interactions in $\text{Ca}_{1.65-2x}\text{Sr}_{0.35}\text{SiO}_4:x\text{Ce}^{3+},x\text{Li}^+$ phosphors.

3.3. Photoluminescence Properties and Energy Transfer of $\text{Eu}^{2+}/\text{Ce}^{3+}/\text{Li}^+$ -Codoped $\text{Ca}_{1.65}\text{Sr}_{0.35}\text{SiO}_4$ Phosphors. The PLE and PL spectra of $\text{Ca}_{1.59}\text{Sr}_{0.35}\text{SiO}_4:0.03\text{Ce}^{3+},0.03\text{Li}^+$ are presented in Figure 7a for comparison. A significant spectral overlap between the PL spectrum of $\text{Ca}_{1.59}\text{Sr}_{0.35}\text{SiO}_4:0.03\text{Ce}^{3+},0.03\text{Li}^+$ and the PLE spectrum of $\text{Ca}_{1.65}\text{Sr}_{0.345}\text{SiO}_4:0.005\text{Eu}^{2+}$ is observed. As a result, energy transfer from Ce^{3+} to Eu^{2+} ions is expected to occur in the $\text{Ca}_{1.65}\text{Sr}_{0.35}\text{SiO}_4$ system.²⁰ As also depicted in Figure 7b, the PL spectrum of Eu^{2+} singly doped $\text{Ca}_{1.65}\text{Sr}_{0.35}\text{SiO}_4$ phosphor shows a broad emission band centered at 538 nm due to the typical $4f^65d^1-4f^7$ transition of Eu^{2+} , and the PLE spectrum shows a broad absorption from 260 to 480 nm with a maximum at 365 nm. To confirm the phenomenon, Figure 7c depicts the PLE and PL spectra $\text{Ca}_{1.59}\text{Sr}_{0.345}\text{SiO}_4:0.03\text{Ce}^{3+},0.03\text{Li}^+,0.005\text{Eu}^{2+}$ phosphors. According to the spectra, the phosphor simultaneously shows a green emission band of Eu^{2+} ions and a blue emission band of Ce^{3+} ions upon excitation at 365 nm. When monitored at 465 and 538 nm, the PLE spectral profiles are similar, and the peaks are both located at about 365 nm, which also provides evidence for resonance energy transfer from Ce^{3+} to Eu^{2+} . Consequently, Ce^{3+} and Eu^{2+} codoped into the $\text{Ca}_{1.65}\text{Sr}_{0.35}\text{SiO}_4$ lattice function as the energy donor and energy acceptor, respectively.

Therefore, a series of phosphors with fixed Ce^{3+} content and varying Eu^{2+} content were prepared to study the effect of doping concentration on the luminescence properties of phosphors. Based on the above analysis, the Ce^{3+} concentration was fixed at 0.03 , and the concentration of Eu^{2+} was varied. Figure 8a,b shows the as-measured and normalized PL spectra of the $\text{Ca}_{1.59}\text{Sr}_{0.35-x}\text{SiO}_4:0.03\text{Ce}^{3+},0.03\text{Li}^+,x\text{Eu}^{2+}$ ($x = 0, 0.001, 0.005, 0.008, 0.010, 0.015$, and 0.020) phosphors under UV excitation ($\lambda_{\text{ex}} = 365$ nm). From Figure 8a, it can be clearly seen that the Ce^{3+} emission decreases sharply, whereas the Eu^{2+} emission increases gradually, and the total emission intensity decreases obviously, suggesting energy transfer from Ce^{3+} to Eu^{2+} . In Figure 8b, one can see that, with increasing Eu^{2+} concentration, the emission spectrum exhibits a red-shift behavior as a result of the decreased Ce^{3+} emission and increased Eu^{2+} emission. Therefore, the observed emission peak shifts from 465 to nearly 550 nm, and the phosphor color is tuned from blue to green, which also strongly verifies the energy transfer from Ce^{3+} to Eu^{2+} . Herein, the critical distance for concentration quenching, R_c , was calculated according to the equation²¹

$$R_c \approx 2 \left(\frac{3V}{4\pi x_c N} \right)^{1/3} \quad (2)$$

where V is the volume of the unit cell, N is the number of ions per unit cell, and x_c is the optimum doping content of activator ions. For the $\text{Ca}_{1.65}\text{Sr}_{0.45}\text{SiO}_4$ host lattice, $N = 12$; $V = 1071.03$ Å; and $x_c = 0.035$, which corresponds to the sum of the Ce^{3+} concentration of 0.03 and the critical Eu^{2+} concentration of 0.005 . The critical distance R_c was determined to be 17.0 Å,

showing that the energy-transfer mechanism in this system is governed by a multipolar interaction. Therefore, based on Dexter's energy-transfer formula for multipolar interactions and the Reisfeld approximation, the possible multipolar interaction in the present system can be calculated as²²

$$\frac{I_{S0}}{I_S} \propto C^{n/3} \quad (3)$$

where I_{S0} and I_S are the luminescence intensities of the sensitizer Ce^{3+} in the presence and absence, respectively, of activator Eu^{2+} and the concentration C is the sum of the Ce^{3+} and Eu^{2+} concentrations. Plots of I_{S0}/I_S versus $C^{n/3}$ with $n = 6, 8$, and 10 correspond to dipole–dipole (d–d), dipole–quadrupole (d–q), and quadrupole–quadrupole (q–q) interactions, respectively. The dependence of I_{S0}/I_S of Eu^{2+} on $C^{6/3}$, $C^{8/3}$, and $C^{10/3}$ is illustrated in Figure 9, and a linear behavior can be observed only for $n = 10$. This clearly indicates that the energy transfer from Ce^{3+} to Eu^{2+} follows a quadrupole–quadrupole interaction.²³

An investigation of the luminescence dynamics can provide more information on the energy-transfer process, so we measured the PL decay curves of Ce^{3+} in $\text{Ca}_{1.59}\text{Sr}_{0.35-x}\text{SiO}_4:0.03\text{Ce}^{3+},0.03\text{Li}^+,x\text{Eu}^{2+}$ phosphors. Figure 10a shows the decay curves of Ce^{3+} emission in $\text{Ca}_{1.59}\text{Sr}_{0.35-x}\text{SiO}_4:0.03\text{Ce}^{3+},0.03\text{Li}^+,x\text{Eu}^{2+}$ phosphors under excitation at 365 nm, as monitored at 465 nm. Second-order exponential decay curves were found that can be fitted by the equation²⁴

$$I(t) = I_0 + A_1 \exp(-t/\tau_1) + A_2 \exp(-t/\tau_2) \quad (4)$$

where t is the time; A_1 and A_2 are constants; $I(t)$ is the luminescence intensity at time t ; and τ_1 and τ_2 are the fast and slow times, respectively, for the exponential components. Then, we calculated the average lifetime τ^* as

$$\tau^* = (A_1\tau_1^2 + A_2\tau_2^2)/(A_1\tau_1 + A_2\tau_2) \quad (5)$$

The calculated average lifetime values for Ce^{3+} ions were determined to be $38.03, 35.88, 29.03, 18.33, 17.55, 13.83$, and 12.11 ns for Eu^{2+} concentrations (x) of $0, 0.001, 0.005, 0.008, 0.015$, and 0.020 , respectively. Obviously, the lifetime values decreased monotonically as the Eu^{2+} concentration increased, which strongly demonstrates energy transfer from Ce^{3+} to Eu^{2+} . The energy-transfer efficiency, η_T , between the Ce^{3+} and Eu^{2+} ions was also obtained from the decay lifetime by using the equation^{25,26}

$$\eta_T = 1 - \frac{\tau_x}{\tau_0} \quad (6)$$

where τ_x and τ_0 are the lifetimes of the Ce^{3+} sensitizer in the presence and absence, respectively, of activator (Eu^{2+}).⁶ The dependences of the Ce^{3+} fluorescence lifetime (monitored at 465 nm) and the energy-transfer efficiency on the doped Eu^{2+} molar concentration in $\text{Ca}_{1.59}\text{Sr}_{0.35-x}\text{SiO}_4:0.03\text{Ce}^{3+},0.03\text{Li}^+,x\text{Eu}^{2+}$ samples are shown in Figure 10b. From the curves, one can see that the average lifetime decreased monotonically and the energy-transfer efficiency increased gradually with the increment of the Eu^{2+} content. The η_T value reached the maximum of 68.15% at $n = 0.020$, indicating that the energy transfer from Ce^{3+} to Eu^{2+} is efficient.

The quantum efficiency (QE) of the selected $\text{Ca}_{1.59}\text{Sr}_{0.27}\text{SiO}_4:0.03\text{Ce}^{3+},0.03\text{Li}^+,0.08\text{Eu}^{2+}$ phosphor was measured using an integrating sphere. As demonstrated in Figure 11,

the internal QE value can be calculated according to the equation⁵

$$\eta_{QE} = \frac{\int L_S}{\int E_R - \int E_S} \quad (7)$$

where L_S is the luminescence emission spectrum of the sample, E_S is the spectrum of the light used for exciting the sample, and E_R is the spectrum of the excitation light without the sample in the sphere. The internal QE of the $\text{Ca}_{1.59}\text{Sr}_{0.27}\text{SiO}_4:\text{0.03Ce}^{3+},\text{0.03Li}^+,0.08\text{Eu}^{2+}$ phosphor under 365-nm excitation was determined to be 45.17%. Figure 12 shows the chromaticity diagram and a series of digital photographs of the selected $\text{Ca}_{1.59}\text{Sr}_{0.35-x}\text{SiO}_4:\text{0.03Ce}^{3+},\text{0.03Li}^+,x\text{Eu}^{2+}$ ($x = 0, 0.001, 0.005, 0.008, 0.015$, and 0.020) phosphors ($\lambda_{ex} = 365$ nm). The CIE results are listed in Table 3. From Figure 12, one can see that the emission colors of $\text{Ca}_{1.59}\text{Sr}_{0.35-x}\text{SiO}_4:\text{0.03Ce}^{3+},\text{0.03Li}^+,x\text{Eu}^{2+}$ phosphors can be shifted from blue to green by adjusting the Eu^{2+} doping level. Accordingly, the corresponding CIE coordinates of $\text{Ca}_{1.59}\text{Sr}_{0.35-x}\text{SiO}_4:\text{0.03Ce}^{3+},\text{0.03Li}^+,x\text{Eu}^{2+}$ can be changed from $(0.148, 0.138)$ to $(0.289, 0.466)$ by changing the different emission compositions of the Ce^{3+} and Eu^{2+} ions. Also, on the right side, one can see the red shift from the color spectra (Figure 12b,c). Based on these results, it is clear that these blue-green $\text{Ca}_{1.59}\text{Sr}_{0.35-x}\text{SiO}_4:\text{0.03Ce}^{3+},\text{0.03Li}^+,x\text{Eu}^{2+}$ phosphors can be efficiently excited in the UV range. It indicates that $\text{Ca}_{1.59}\text{Sr}_{0.35-x}\text{SiO}_4:\text{0.03Ce}^{3+},\text{0.03Li}^+,x\text{Eu}^{2+}$ phosphors can act as potential blue-green tunable phosphors for possible applications in the solid-state lighting (SSL) industry.

4. CONCLUSIONS

In conclusion, novel Eu^{2+} and $\text{Ce}^{3+}/\text{Li}^+$ singly doped and $\text{Eu}^{2+}/\text{Ce}^{3+}/\text{Li}^+$ -codoped $\text{Ca}_{1.65}\text{Sr}_{0.35}\text{SiO}_4$ phosphors have been prepared by a high-temperature solid-state reaction. The crystal structure of $\text{Ca}_{1.65}\text{Sr}_{0.35}\text{SiO}_4$ was identified as that of the $\alpha'_L\text{-Ca}_2\text{SiO}_4$ phase based on Rietveld refinement analysis. Eu^{2+} and $\text{Ce}^{3+}/\text{Li}^+$ dopants were determined to occupy the specific crystallographic positions of $\text{Sr}^{2+}/\text{Ca}^{2+}$, depending on the variation of the cell volumes and chemical compositions of the isostructural $\text{Ca}_{2-x}\text{Sr}_x\text{SiO}_4$ ($x = 0.25, 0.35, 0.45, 0.55, 0.65$) compounds. The color-tunable $\text{Ca}_{1.65}\text{Sr}_{0.35}\text{SiO}_4:\text{Ce}^{3+},\text{Li}^+,\text{Eu}^{2+}$ phosphors exhibit strong absorption in the range of 250–450 nm, and the emission color of the phosphors can be tuned appropriately from blue (0.148, 0.138) to green (0.289, 0.466) with increasing Eu^{2+} concentration. The energy-transfer efficiency between Ce^{3+} and Eu^{2+} determined from decay curves reached a maxim of 68.15% for an Eu^{2+} doping content of 0.02. The results indicate that $\text{Ca}_{1.65}\text{Sr}_{0.35}\text{SiO}_4:\text{Ce}^{3+},\text{Li}^+,\text{Eu}^{2+}$ phosphors might have potential applications in near-UV-pumped WLEDs.

■ AUTHOR INFORMATION

Corresponding Author

*E-mail: xiazg@ustb.edu.cn. Tel.: +86-10-8237-7955. Fax: +86-10-8237-7955.

Notes

The authors declare no competing financial interest.

■ ACKNOWLEDGMENTS

The present work was supported by the National Natural Science Foundations of China (Grants 51002146, 51272242); Natural Science Foundations of Beijing (2132050); the

Program for New Century Excellent Talents in the University of the Ministry of Education of China (NCET-12-0950); the Beijing Nova Program (Z131103000413047); the Beijing Youth Excellent Talent Program (YETP0635); the Funds of the State Key Laboratory of New Ceramics and Fine Processing, Tsinghua University (KF201306); and the Fundamental Research Funds for the Central Universities (FRF-TP-14-005A1).

■ REFERENCES

- Xia, Z. G.; Zhang, Y. Y.; Molokeev, M.; Atuchin, V. V.; Luo, Y. *Sci. Rep.* **2013**, *3*, 3310.
- Kalaji, A.; Mikami, M.; Cheetham, A. K. *Chem. Mater.* **2014**, *26*, 3966–3975.
- Lin, C. C.; Liu, R. S. *J. Phys. Chem. Lett.* **2011**, *11*, 1268–1277.
- Li, G. G.; Lin, C. C.; Chen, W. T.; Molokeev, M. S.; Atuchin, V. V.; Chiang, C. Y.; Zhou, W. Z.; Wang, C. W.; Li, W. H.; Sheu, H. S.; Chan, T. S.; Ma, C. G.; Liu, R. S. *Chem. Mater.* **2014**, *26*, 2991–3001.
- Miao, S. H.; Xia, Z. G.; Zhang, J.; Liu, Q. L. *Inorg. Chem.* **2014**, *53*, 10386–10393.
- Denault, K. A.; Brögch, J.; Gaultois, M. W.; Mikhailovsky, A.; Petry, R.; Winkler, H.; DenBaars, S. P.; Seshadri, R. *Chem. Mater.* **2014**, *26*, 2275–2282.
- Jang, H. S.; Kim, H. Y.; Kim, Y. S.; Lee, H. M.; Jeon, D. Y. *Opt. Express* **2012**, *20*, 2761–2771.
- Hao, Z. D.; Zhang, J. H.; Zhang, X.; Luo, Y. S.; Zhang, L. G.; Zhao, H. F. *J. Lumin.* **2014**, *152*, 40–43.
- Li, Y. Y.; Wu, Q. S.; Wang, X. C.; Ding, J. Y.; Long, Q.; Wang, Y. H. *RSC Adv.* **2014**, *4*, 63569–63575.
- Chen, H.; Li, C. X.; Hua, Y. J.; Yu, L. L.; Jiang, Q. Y.; Deng, D. G.; Zhao, S. L.; M, H. P.; Xu, S. Q. *Ceram. Int.* **2014**, *40*, 1979–1983.
- Shang, M. M.; Li, G. G.; Geng, D. L.; Yang, D. M.; Kang, X. J.; Zhang, Y.; Lian, H. Z.; Lin, J. *J. Phys. Chem. C* **2012**, *116*, 10222–10231.
- Chen, L.; Luo, A. Q.; Zhang, Y.; Liu, F. Y.; Jiang, Y.; Xu, Q. S.; Chen, X. H.; Hu, Q. Z.; Chen, S. F.; Chen, K. J.; Kuo, H. C. *ACS Comb. Sci.* **2012**, *14*, 636–644.
- Barbier, J.; Hyde, B. G. *Acta Crystallogr. B* **1985**, *41*, 383–390.
- Mumme, W. G.; Cranswick, L.; Chakoumakos, B. *Neues Jahrb. Mineral.* **1996**, *170*, 171–188.
- Shannon, R. D. *Acta Crystallogr. A* **1976**, *32*, 751–767.
- Li, G. G.; Zhang, Y.; Geng, D. L.; Shang, M. M.; Peng, C.; Cheng, Z. Y.; Lin, J. *ACS Appl. Mater. Interfaces* **2012**, *4*, 296–305.
- Lv, W.; Guo, N.; Jia, Y. C.; Zhao, Q.; Lv, W. Z.; Jiao, M. M.; Shao, B. Q.; You, H. P. *Inorg. Chem.* **2013**, *52*, 3007–3012.
- Xia, Z. G.; Liu, R. S. *J. Phys. Chem. C* **2012**, *116*, 15604–15609.
- Che, Y.; Li, Y.; Wang, J.; Wu, M. M.; Wang, C. X. *J. Phys. Chem. C* **2014**, *118*, 12494–12499.
- Chengaiah, T.; Jayasankar, C. K.; Moorthy, L. R. *Phys. B* **2013**, *431*, 137–141.
- Li, Y. Y.; Shi, Y. R.; Zhu, G.; Wu, Q. S.; Li, H.; Wang, X. C.; Wang, Q.; Wang, Y. H. *Inorg. Chem.* **2014**, *53*, 7668–7675.
- Li, G. G.; Geng, D. L.; Shang, M. M.; Zhang, Y.; Peng, C.; Cheng, Z. Y.; Lin, J. *J. Phys. Chem. C* **2011**, *115*, 21882–21892.
- Xia, Z. G.; Liu, R. S.; Huang, K. W.; Drozd, V. J. *Mater. Chem.* **2012**, *22*, 15183–15189.
- Jiao, M. M.; Guo, N.; Lv, W.; Jia, Y. C.; Lv, W. Z.; Zhao, Q.; Shao, B. Q.; You, H. P. *Inorg. Chem.* **2013**, *52*, 10340–10346.
- Geng, D. L.; Lian, H. Z.; Shang, M. M.; Zhang, Y.; Lin, J. *Inorg. Chem.* **2014**, *53*, 2230–2239.
- Xia, Z. G.; Wu, W. W. *Dalton Trans.* **2013**, *42*, 12989–12997.